Photocurable Oil/Water Interfaces as a Universal Platform for 2-D Self-Assembly†

Jason J. Benkoski,* Ronald L. Jones, Jack F. Douglas, and Alamgir Karim

Polymers Division, National Institute of Standards and Technology, Gaithersburg, Maryland 20899

Received July 28, 2006. In Final Form: December 14, 2006

We present a novel platform, dubbed fossilized liquid assembly, for the creation of 2-D assemblies from nanoscale building blocks. The system consists of an oil/water interface in which the oil phase can be flash-cured upon UV exposure. The photopolymerizable material, 1,12-dodecanediol dimethacrylate, solidifies in as little as 1 s when exposed to UV light. The rapid cross-linking allows one to obtain a "snapshot" of the assembly process for particles that segregate to the oil/water interface. Among the particles investigated were nonpolar 0.39 μm poly(methyl methacrylate) latex spheres, nonpolar 10 μm polystyrene latex spheres, highly polarizable 5 nm Au nanocrystals, dipolar 10 nm CdTe quantum dots, and magnetic 25 nm magnetite nanoparticles. The aggregates formed by this process were typically either globular or fractal in appearance. By comparing with simulation, we can perform quantitative image analysis on the resulting micrographs to define a rigorous set of standards for distinguishing among the main classes of aggregation: flocculation, equilibrium phase separation, and true self-assembly.

Introduction

Self-assembly is an attractive complement to lithography for the fabrication of nanodevices and nanostructured materials due to its inherent simplicity, flexibility, and low cost. Living organisms have successfully exploited this phenomenon to create naturally occurring nanotechnologies such as encapsulation,[1,2] mechanical scaffolding,[3,4] and photosynthetic assemblies.[5,6] By applying the same strategies to synthetic building blocks, self-assembly holds great promise for rapid, reproducible production of highly complex structures down to nanometer-length scales. Unfortunately, studies of nanoparticle self-assembly are plagued by the difficulties involved with directly observing the assembly process at such small size scales. Microscopy techniques, in particular, require tedious sample preparation steps that often introduce artifacts. Common sample preparation procedures, such as dip coating, spin casting, water vitrification, and microtomy, can often make it difficult to distinguish between nonequilibrium aggregation mechanisms such as flocculation and true self-assembly.

Although used in a variety of contexts, self-assembly is defined here as reversible, spontaneous organization into predefined structures where the blueprint of the final geometry is coded directly into the interaction potentials of the component building blocks. The classic examples of self-assembly are the tobacco mosaic virus, actin filaments, and surfactant micelles. In these and other examples, the blueprint is coded into the building blocks through directional bonds, such as dipolar bonds, or through a combination of bonds having a specific spatial registry (lock-and-key interactions).

To visualize submicrometer aggregates while minimizing the perturbation to the assembly process, we have developed a novel platform, called fossilized liquid assembly (FLA), for the creation of nanoscale assemblies in two dimensions. It consists of an oil/water interface, where the oil phase can be flash-cured to form a rigid polymer when exposed to UV light. The surface of the cured film therefore preserves a "snapshot" of the 2-D assembly at the instant of UV exposure.[7] Fossilized liquid assembly offers many advantages over other strategies for imaging self-assembly at the nanoscale level: (i) The high interfacial tension of the oil/water interface provides a strong driving force for interfacial segregation for almost any type of particle. (ii) The lateral mobility of the liquid/liquid interface makes it possible for particles to assemble under equilibrium conditions and anneal continuously. (iii) The reduced dimensionality makes it practical to observe all particle densities from very dilute concentrations up to closest packing. (iv) Perhaps most unique to this platform is the preservation of the assemblies by rapid cross-linking, which overcomes the limitations of atomic force microscopy (AFM) and scanning electron microscopy (SEM) with respect to imaging small and highly mobile structures at a liquid/liquid interface.

Using an oil/water interface as a platform for self-assembly is not without its complications, however. One example is the well-documented dipole moment that arises in charged particles at the oil/water or air/water interface.[8−10] This phenomenon is explained by the asymmetric counterion cloud that forms on the water side of the interface. Since it is not balanced by an equivalent counterion cloud in the hydrophobic phase, it results in a net electric dipole that points toward the aqueous phase. The particles therefore repel each other through the hydrophobic phase with an algebraic, dipolar force law. Observe that this repulsive force acts isotropically in the plane of the interface, much as the van

† Official contribution of the National Institute of Standards and Technology; not subject to copyright in the United States.

* To whom correspondence should be addressed. E-mail: jason.benkoski@jhuapl.edu.

(1) Zandi, R.; van der Schoot, P.; Reguera, D.; Kegel, W.; Reiss, H. *Biophys. J.* **2006**, *90*, 1939.

(2) Chen, C.; Kwak, E. S.; Stein, B.; Kao, C. C.; Dragnea, B. *J. Nanosci. Nanotechnol.* **2005**, *5*, 2029.

(3) Hurtley, S. M. *Science* **1998**, *279*, 459.

(4) Forgacs, G.; Newman, S. A.; Hinner, B.; Maier, C. W.; Sackmann, E. *Biophys. J.* **2003**, *84*, 1272.

(5) Deisenhofer, J.; Epp, O.; Miki, K.; Huber, R.; Michel, H. *J. Mol. Biol.* **1984**, *180*, 385.

(6) Drews, G. *Microbiol. Rev.* **1985**, *49*, 59.

(7) As described in later sections, the oil phase initially has a viscosity of 15 mPa•s and becomes completely solidified in less than 1 s. The sample geometry is such that the growth front of radical polymerization proceeds from the oil/water interface downward to the bulk oil film. We believe that the viscosity rises continuously from 15 mPa•s to infinity during this time, which should gradually slow the particle dynamics but not alter the size or morphology of the final aggregate.

(8) Pieranski, P. *Phys. Rev. Lett.* **1980**, *45*, 569.

(9) Reynaert, S.; Moldenaers, P.; Vermant, J. *Langmuir* **2006**, *22*, 4936.

(10) Hurd, A. J. *J. Phys. A: Math. Gen.* **1985**, *18*, L1055.

10.1021/la062230i
Published on Web 02/21/2007

der Waals attraction is isotropic. It should therefore act together with thermal energy to favor the dispersed state without imposing any signature pattern, or artifact, on the aggregate morphologies. Unfortunately, surface charges still add significant complications to the interpretation of the aggregation process at oil/water interfaces. Other complications introduced by surface charges include unscreened charges adjacent to the oil phase and electrocapillary effects.[11−14] Fortunately, the vast body of work in this area[8−10,15−19] ensures that successful strategies can be enacted to minimize these spurious effects either through sample geometry, particle shape, or processing conditions or by avoiding charged particles altogether.

The current platform therefore builds upon these previous attempts at using fluid/fluid interfaces for self-assembly. Though the fixation of nanoparticle aggregates has been achieved by solvent casting onto solid substrates,[20−23] by direct particle binding,[24,25] and by gelation of the aqueous phase,[26−28] the current platform is the first example, to our knowledge, of irreversible fixation performed through the oil phase. Therefore, the focus of this paper is to investigate different forms of particle aggregation by observing model systems that involve equivalent particles. Having demonstrated the ability to facilitate equilibrium self-assembly, we further set out to define a set of rigorous standards for distinguishing among the main categories of aggregation, namely, flocculation, phase separation, and true self-assembly. Using quantitative image analysis, we attempt to classify the aggregation mechanism by comparing the experimentally obtained micrographs with the appropriate theoretical models.

Results

Samples were prepared for 2-D particle aggregation in the configuration shown in Figure 1. Experiments were carried out on particles having a variety of sizes and compositions to investigate the effects of different types of interactions. In all, five different particles were successfully deposited at the 1,12-dodecanediol dimethacrylate (DDMA)/water interface: 0.39 μm uncharged poly(methyl methacrylate) (PMMA) particles, 10 μm uncharged polystyrene (PS) particles, 5 nm negatively charged Au nanoparticles, 9 nm CdTe quantum dots coated with 5000 g/mol grafted poly(ethylene glycol) (PEG) chains, and 25 nm magnetite nanoparticles with no surface functionalization. These

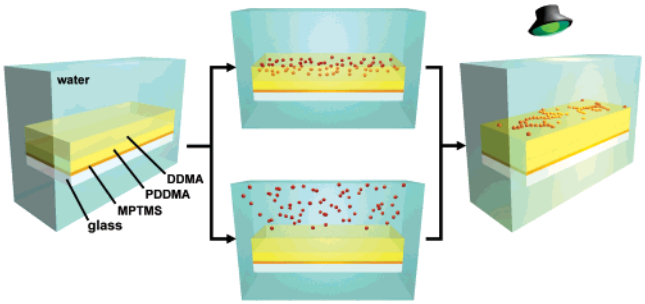

Figure 1. Schematic diagram of self-assembly samples showing DDMA-coated glass slides immersed in water. The nanoparticles could be dispersed initially in either the oil or water phase, depending on which gave better results. Once the particles are given time to segregate to the interface and self-assemble, the assembly is "frozen" by cross-linking the DDMA with UV light.

particles were chosen since they exhibit interaction potentials having different interparticle symmetries, a property identified as crucially important in controlling the form of self-assembled structures.[29,30]

In the case of the 0.39 μm PMMA particles and 10 μm PS particles, we could observe two nonpolar systems having primarily van der Waals attraction and hard core repulsion. The difference in size allowed us to view the effects of increasing the strength of the dispersion interaction. The 5 nm Au nanoparticles allowed us to view the effects of increasing the van der Waals attraction by choosing a more polarizable material. Finally, the CdTe quantum dots and magnetite nanoparticles possessed both van der Waals and dipolar attractions. The relative strengths of these potentials differed in these two systems, allowing us to observe how the competition between a directional (dipolar) potential and an isotropic (van der Waals) potential affects the ability of the particles to self-assemble into well-defined structures such as loops or linear chains.

Figure 2a is an AFM micrograph showing the aggregation of 0.39 μm PMMA particles at the oil/water interface. The bulk concentration of the particles varied continuously from 5% to 0% by mass fraction in the DDMA phase. Note the lack of agglomeration, which was evident even at high concentrations. To a first approximation, two 0.39 μm PMMA spheres in intimate contact would have a van der Waals attraction of at least $-100k_BT$.[31,32] Surprisingly, the particles did not aggregate when placed at the DDMA/water interface. The observed particle dispersion is essentially a 2-D gas. The 0.39 μm PMMA particles, which were synthesized via a standard emulsion polymerization, possess no surface charge to our knowledge. Unfortunately, ζ-potential measurements and conductometric titrations could not be performed due to the complete lack of solubility in water. We therefore attempted to test the possibility of surface charge by preparing additional samples with various particle concentrations in the presence of a buffered saline solution containing 1.5 mol/L $CaCl_2$. Even after 2 h, we observed no noticeable

(11) Nikolaides, M. G.; Bausch, M. G.; Hsu, M. F.; Dinsmore, A. D.; Brenner, M. P.; Weitz, D. A. *Nature* **2002**, *420*, 299.
(12) Nikolaides, M. G.; Bausch, M. G.; Hsu, M. F.; Dinsmore, A. D.; Brenner, M. P.; Weitz, D. A. *Nature* **2003**, *424*, 1014.
(13) Danov, K. D.; Kralchevsky, P. A.; Boneva, M. P.; *Langmuir* **2004**, *20*, 6139.
(14) Megen, M.; Aizenberg, J. *Nature* **2003**, *424*, 1014.
(15) Stamou, D.; Duschl, C.; Johannsmann, D. *Phys. Rev. E* **2000**, *62*, 5263.
(16) Stankiewicz, J.; Cabrerizo, M. A.; Cabrerizo, Vílchez, M. A.; Hidalgo, Alvarez, R. *Phys. Rev. E* **1993**, *47*, 2663.
(17) Doroszkowski, A.; Lambourne, R. *J. Polymer. Sci., Part C: Polym. Symp.* **1971**, *34*, 253.
(18) Aveyard, R.; Clint, J. H.; Nees, D.; Paunov, V. N. *Langmuir* **2000**, *16*, 1969.
(19) Horozov, T. S.; Avayard, R.; Clint, J. H.; Neumann, B. *Langmuir* **2005**, *21*, 2330.
(20) Ge, G.; Brus, L. *J. Phys. Chem. B* **2000**, *104*, 9573.
(21) Tang, J.; Ge, G.; Brus, L. E. *J. Phys. Chem. B* **2002**, *106*, 5653.
(22) Rabani, E.; Relchman, D. R.; Geissler, P. L.; Brus, L. E. *Nature* **2003**, *426*, 271.
(23) Sztrum, C. G.; Hod, O.; Rabani, E. *J. Phys. Chem. B* **2005**, *109*, 6741.
(24) Lin, Y.; Skaff, H.; Emrick, T.; Dinsmoe, A. D.; Russell, T. P. *Science* **2003**, *299*, 226−229.
(25) Russell, J. T.; Lin, Y.; Böker, A.; Su, L.; Carl, P.; Zettl, H.; He, J.; Sill, K.; Tangirala, R.; Emrick, T.; Littrell, K.; Thiyagarajan, P.; Cookson, D.; Fery, A.; Wang, Q.; Russell, T. P. *Angew. Chem., Int. Ed.* **2005**, *44*, 2420.
(26) Paunov, V. N. *Langmuir* **2003**, *19*, 7970.
(27) Duan, H.; Wang, D.; Sobal, N. S.; Giersig, M.; Kurth, D. G.; Möhwald, H. *Nano Lett.* **2005**, *5*, 949.
(28) Wang, D.; Duan, H.; Möhwald, H. *Soft Matter* **2005**, *1*, 412.
(29) van Workum, K.; Douglas, J. F. *Macromol. Symp.* **2005**, *227*, 1.
(30) van Workum, K.; Douglas, J. F. *Phys. Rev. E* **2005**, *71*, 031502.
(31) The van der Waals interaction energy (E_{vdW}) for two particles is given by $E_{vdW} = -A_H a/12D$, where A_H is the Hamaker constant, a is the particle radius, D is the separation distance, and $D \ll a$. To a first approximation, $D \approx 0.2$ nm, $a = 195$ nm, and $A_H \approx 1 \times 10^{-20}$ J for PMMA acting across water.[32] Since A_H is much smaller for PMMA interacting across DDMA, we can estimate the upper limit of E_{vdW} to be no more than $-200k_BT$. The complications of calculating the attractive interactions along an interface and the uncertainty of A for PMMA across DDMA make the lower limit more difficult to evaluate. Nevertheless, the interaction between identical particles is always attractive regardless of the intervening medium. We can therefore suggest a lower limit of $-100k_BT$, which is half the value for PMMA spheres in water.
(32) Israelachvili, J. *Intermolecular & surface forces*; Academic Press Inc.: San Diego, CA, 1992; p 315.

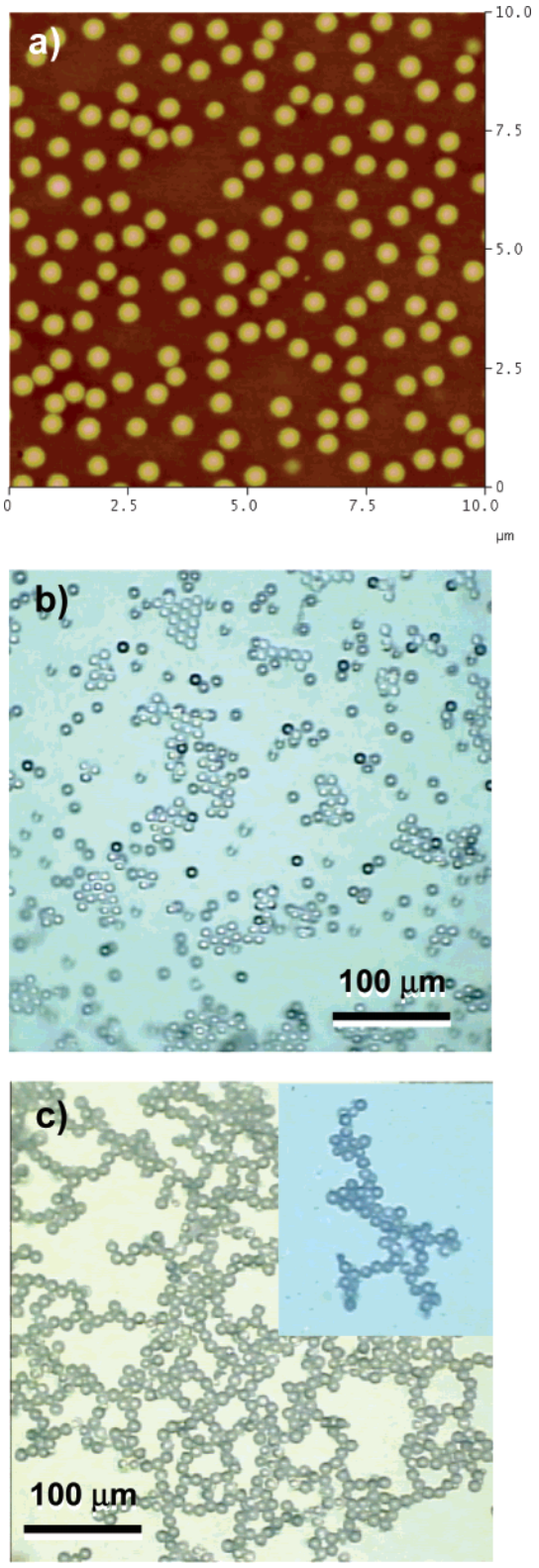

Figure 2. Assembly of nonpolar polymer latex particles: (a) AFM micrographs of 0.39 μm PMMA spheres, (b) an optical micrograph of 10 μm surfactant-coated PS deposited from the aqueous phase, and (c) an optical micrograph of 10 μm bare PS deposited from the oil phase. The inset in (c) shows an isolated aggregate that was found in between two very large aggregates. The *z*-scale in (a) is 250 nm.

agglomeration for all particle densities, from very dilute concentrations up to 25% areal coverage. One should note, however, that a small residual electric charge at the particle/oil interface has been proposed to explain the commonly observed long-range repulsions between charged latex spheres at the oil/water interface.[33,34] These studies noted many cases where the interparticle repulsion was insensitive to the ionic strength of the aqueous phase.

In addition to thermal energy and electrostatic repulsion, dispersion may also be aided by the steric repulsion of solvated PMMA chains at the particle surfaces. The degree of cross-linking was sufficient to maintain the overall shape of the particles, but they were no doubt swollen by the DDMA to some extent. Since only a portion of the particles are exposed at the interface, a precise determination of the amount of swelling is difficult. However, the minimum center-to-center spacing of two particles in close contact typically measures ~0.43 μm rather than 0.39 μm. This 10% increase in the diameter suggests that the interaction between DDMA and PMMA may be favorable enough to result in steric stabilization due to the aforementioned corona of solvated chains.

Figure 2b is an optical micrograph showing a similar assembly of 10 μm surfactant-coated PS particles (Kisker Biotech[35]) that were deposited from the aqueous phase and allowed to aggregate at 20 °C for 1 h. The as-received particles are stabilized in water through a proprietary formulation of electrically neutral surfactants. Since the particles are roughly 20 times larger than the PMMA particles and have a similar dielectric constant, the van der Waals attraction would be expected to be about 20 times as large. Offsetting this increased attraction is the steric stabilization from the surfactant coating. One can then contrast the amount of aggregation with that shown in Figure 2a. As a further comparison, the surfactant layer was stripped from the PS particles by first drying the as-received aqueous suspension and then rinsing the particle residue with dichloroethane. The PS particles were then resuspended in the DDMA, and the above experiment was repeated. Observe in Figure 2c how highly branched the aggregates are for the uncoated particles. This dramatic change in the aggregate morphology appears to be modulated by the repulsive interactions of the surfactant layer.

On a smaller length scale, 5 nm Au nanoparticles (Goldmark Biologicals[35]) formed irregularly shaped aggregates, as shown in Figure 3. The negative surface charge that is used to disperse the Au nanoparticles in aqueous suspension also prevented interfacial segregation when a 100 mmol/L NaCl buffer was used. Switching to 100 mmol/L $CaCl_2$ buffer increased the amount of nanoparticles at the interface, but 60 min was required to see significant flocculation. Note the similarity between Figure 3 and the inset in Figure 2c.

AFM inspection of the Au nanoparticle samples also revealed that larger aggregates formed slight depressions in the oil/water interface. This observation is significant, for it leaves open the possibility that capillary forces may be acting among the aggregates if not the individual particles. Lateral capillary interactions arise due to the overlap of the menisci of adjacent bodies at the interface and can act over relatively large distances.[9,36] Further complicating the analysis is the asymmetry of such interactions when they involve nonspherical bodies.[37,38]

(33) Aveyard, R.; Clint, J. H.; Nees, D.; Paunov, V. N. *Langmuir* **2000**, *16*, 1969.
(34) Aveyard, R.; Binks, B. P.; Clint, J. H.; Fletcher, P. D. I.; Horozov, T. S.; Nermann, B.; Paunov, V. N.; Annesley, J.; Botchway, S. W.; Nees, D.; Parker, A. W.; Ward, A. D.; Burgess, A. N. *Phys. Rev. Lett.* **2002**, *88*, 245102-1.
(35) Certain commercial equipment, instruments, or materials are identified in this paper to specify the experimental procedure adequately. Such identification is not intended to imply recommendation or endorsement by the National Institute of Standards and Technology, nor is it intended to imply that the materials or equipment identified are necessarily the best available for the purpose.
(36) Kralchevsky, P. A.; Nagayama, K. *Langmuir* **1994**, *10*, 23.
(37) Loudet, J. C.; Alsayed, A. M.; Zhang, J.; Yodh, A. G. *Phys. Rev. Lett.* **2005**, *94*, 018301.

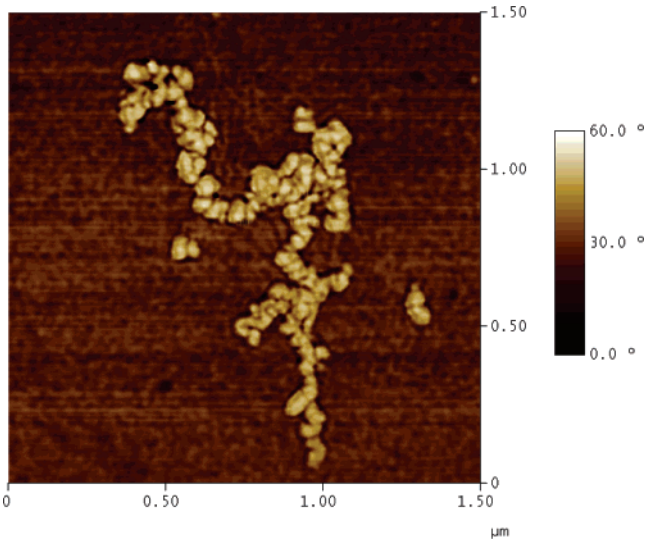

Figure 3. AFM phase image of highly polarizable 5 nm gold nanoparticle assemblies after cross-linking. Due to their negative surface charge, the nanoparticles were deposited from a pH 8 buffer consisting of 100 mmol/L $CaCl_2$ and 10 mmol/L HEPES. The DDMA film was then exposed to the 100 nmol/L nanoparticle suspension for 1 h before cross-linking. For this aggregate, $d_f = 1.57$ and $A = 3.97$.

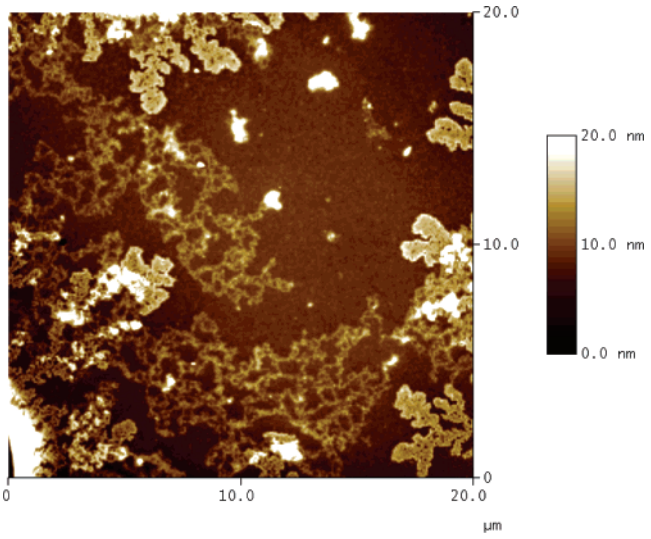

Figure 4. AFM height image of the self-assembly of 9 nm CdTe quantum dots surface modified with PEG. In contrast to polymer latex spheres, the quantum dots self-assemble into much more complex morphologies. The d_f value was calculated to be 1.76, and A was calculated to be 1.25.

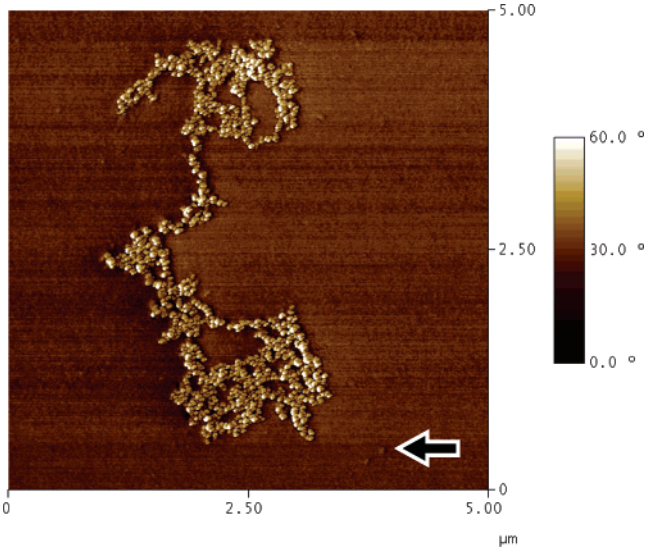

Figure 5. Representative magnetite nanoparticle assembly deposited from a 0.1 nmol/L aqueous suspension. The phase image shows a single, irregularly shaped assembly. The arrow points to one of the few isolated nanoparticles. Although isolated particles do not impose any interfacial curvature, larger assemblies sink due to the effects of gravity. At its deepest point, the assembly sinks ~80 nm below the normal surface level. The calculated value of d_f for this aggregate was 1.60, and A was calculated to be 7.17.

The gravitational pull on a submicrometer particle or aggregate is typically insufficient to generate a significant meniscus,[39] but unfortunately, the menisci are accentuated in the current geometry because the lower density DDMA is actually placed underneath the higher density water. Although some of these effects can be mitigated by aligning the interface parallel to the gravitational field, this particular artifact does not alter the major implications of this study. For a fuller discussion of capillary forces between colloidal particles, one can refer to refs 9 and 36.

CdTe quantum dots (Quantum Dot Corporation[35]) also aggregated at the oil/water interface. The hard core diameter of the particles is 9 nm, but in aqueous suspension, the particles have a 55 nm outer diameter due to their coating of 5000 g/mol poly(ethylene glycol) (PEG). As in the previous example, they were deposited for 60 min from the aqueous phase, which had a concentration of 100 nmol/L. As shown in Figure 4, these particles organize into irregularly shaped networks with a spongelike appearance.

Similar in appearance are assemblies of 25 nm magnetite nanoparticles (Aldrich[35]), shown in Figure 5. The particles were deposited from the aqueous phase with an initial bulk concentration of 0.1 nmol/L. Not shown are optical micrographs demonstrating the reversible alignment of the magnetite assemblies in the presence of an external magnetic field (Supporting Information, Figure S1). For the first experiment, assembly was allowed to occur for 15 min in the absence of an external field, and a bar magnet was then placed under the sample chamber. Although complete alignment did not occur until after 5 min, significant alignment was observed after only 30 s. Similarly, aggregates that formed initially with an external magnetic field for 15 min became randomly oriented and irregularly shaped after only 30 s. The irregularity of the conformations became even more apparent after 5 min without an external field. The extent of the reorganization was striking, particularly given the diameter of the larger aggregates (> 100 μm). Since reversibility is one of the key characteristics of self-assembly, the ability of such large aggregates to rapidly reorganize in response to an external field is encouraging.

Also notable was the fact that few isolated magnetite nanoparticles could be found at the interface. Generally, even the assemblies were spaced by 10 μm or more. This observation suggests that aggregation may occur at a much greater rate than particle deposition. It is more likely, however, that some aggregation occurs in the aqueous phase, followed by interfacial capture. This hypothesis is supported by the observation of nonplanar (three-dimensional) aggregates on samples when the magnetite nanoparticles were deposited from more concentrated aqueous suspensions. Furthermore, dynamic light scattering experiments performed on the aqueous suspensions with a Brookhaven particle sizer measured an average aggregate size

(38) Loudet, J. C.; Yodh, A. G.; Pouligny, B. *Phys. Rev. Lett.* **2006**, *97*, 018304.
(39) Chan, D. Y. C.; Henry, J. D.; White, L. R. *J. Colloid Interface Sci.* **1981**, *79*, 410.

of 717 nm within 15 min of dispersing the magnetite particles in buffer. Aggregates were visible to the naked eye after 24 h. Note that no aggregation was measured in bulk suspension for any of the other particles used in this study.

Discussion

We have demonstrated the use of DDMA/water interfaces as a useful platform for investigating self-assembly. The primary improvement of this model over previous studies of particles at fluid interfaces (the ability to flash-cure the oil phase) means that the transient structure of the aggregates can be preserved and that subsequent imaging is therefore relatively straightforward. Without the ability to preserve snapshots of the aggregated structures by this process, the rapid movement of the particles would make them impossible to image using a slow scanning technique such as AFM. Optical techniques, of course, are limited in magnification, and transmission electron microscopy involves tedious sample preparation steps that are likely to distort the aggregates and introduce artifacts.

The value of fossilized liquid assembly lies partly in its ability to minimize perturbation of the particle aggregation process. One must therefore closely consider the experimental conditions during the rapid polymerization of the oil phase. Starting from 15 mPa·s, the viscosity of DDMA increases smoothly to the gel point, when the viscosity becomes effectively infinite. The whole process takes less than 1 s. Although 1 s is a relatively short time to achieve a full cure, a nanoparticle actually diffuses over a relatively large distance during this time. Using the Einstein relation,[40] one can calculate the average distance, x, that a particle diffuses in time, t

$$x = \sqrt{\frac{k_B T t}{6\pi\eta a}} \quad (1)$$

where k_B is Boltzmann's constant, T is the temperature, η is the viscosity, and a is the particle radius. For a viscosity of 0.89 mPa·s for water and 15 mPa·s for DDMA, the typical diffusion distance is between 1 and 5 μm for a 10 nm particle. These distances roughly correspond to the sizes of the aggregates observed in this study.

The question, then, is whether the final morphologies are influenced by the fixation process. Notice that the above calculation grossly overestimates the diffusion length by assuming that the viscosity remains at its original value throughout the 1 s cure time. In reality, the viscosity of DDMA is much higher during most of that period. A second issue is whether diffusion during the cure time can lead to distortion of the final aggregate. Unless curing results in local hot spots, lateral heterogeneities during gel formation, convective currents, or a Marangoni effect, a globally uniform increase in viscosity should impose no bias on the diffusion paths that lead to the final structure. Rather, a smooth increase in viscosity should merely result in a gradual slowing of diffusion during the cure time. As for the other possibilities, the small thickness of the oil layer ($\sim$100 μm) and the high thermal conductivity and heat capacity of water help to mitigate thermal sources of flow-induced anisotropy. The high concentration of the photoinitiator and the high intensity of the UV light also help to mitigate chemical sources of heterogeneity. For systems such as this, photocuring generally proceeds as a frontal polymerization in which the conversion profile propagates downward from the illuminated surface as a traveling wave of network solidification through the unpolymerized medium.[41] Nevertheless, additional investigations are currently underway to more closely examine the process of cross-linking in this system.

Perhaps more important than the reduction of artifacts is the versatility of this platform. The high interfacial tension of the oil/water interface has been shown to provide a strong driving force for the segregation of many different particle types despite large differences in charge, polarizability, size, and surface chemistry. It therefore allows one to compare the aggregation of a wide variety of materials under remarkably similar conditions. An important consequence of this flexibility is that general trends can be observed as a function of the particle properties. Two separate issues are apparent: (1) the competition between the attractive potentials and thermal energy and (2) the competition between the different types of attractive potentials. The effects of these two issues on morphology are depicted schematically in Figure 6. Issue (1) corresponds to moving along the x-axis, whereas issue (2) applies to the states within the first quadrant of the graph. With the use of the current platform, we can now experimentally access the conditions needed to produce this rich diversity of morphologies.

For case (1), we can consider what happens when two particles initially come into contact. In the limit of very strong binding, the two particles will bind irreversibly upon first contact and will remain permanently fixed in their original relative orientation. This process describes diffusion-limited cluster aggregation (DLCA) (Figure 6 v3).[42−44] The resulting structures are highly branched and loosely packed. Their distinctive appearance results from the mechanism of DLCA growth, in which the exposed ends of the clusters grow more rapidly than other perimeter sites because the perimeter sites near the center are shadowed by the outer branches.[45] At the other limit, the attractive potential energy is comparable with the thermal energy. In this case, the particles join and leave the cluster with well-defined equilibrium constants that vary with the thermodynamic conditions (Figure 6 v1). These clusters will anneal over time, and the final structures will evolve into those that are most thermodynamically stable. Most common are compact droplets driven by surface tension. For moderately strong, but not irreversible, binding energies, reaction-limited cluster aggregation (RLCA) occurs (Figure 6 v2).[46] In this process, the probability of two particles sticking is lower than that for DLCA, and thus many contacts can be explored before the particles finally adhere.

Each of these three mechanisms results in distinct morphologies. One can distinguish among them by quantifying both the fractal dimension (d_f) and the ratio (A) between the principal radii of gyration (R_i), where $A = \langle R_1^2/R_2^2 \rangle$. The theoretical predictions for the two values are given for DLCA, RLCA, and phase separation in Table 1.[47−49] All values assume isotropic interaction potentials such as van der Waals attraction. A simple comparison can be made between the aggregation of the surfactant-coated 10 μm PS spheres and the Au nanocrystals. Observe how the PS particle clusters (Figure 2b), though small, are relatively compact and symmetrical ($d_f \approx 1$, $A \approx 1$), as

(40) Einstein, A. *Investigations of the Theory of Brownian Movement*; Fürth, R., Ed.; Dover: New York, 1956; pp 36−67.
(41) Warren, J. A.; Cabral, J. T.; Douglas, J. F. *Phys. Rev. E* **2005**, *72*, 021801.
(42) Stauffer, D.; Stanley, H. E. *From Newton to Mandelbrot: a primer in theoretical physics with fractals for the Macintosh*; Springer: Berlin, New York, 1996; Chapter 3.
(43) Ossadnik, P. *Physica A* **1993**, *195*, 319.
(44) Vandewalle, N.; Ausloos, M. *Phys. Rev. E* **1995**, *51*, 597.
(45) Witten, T. A.; Sander, L. M. *Phys. Rev. Lett.* **1981**, *47*, 1400.
(46) Forrest, S. R.; Witten, T. A. *J. Phys. A: Math. Gen.* **1979**, *12*, L109.
(47) Robinson, D. J.; Earnshaw, J. C. *Phys. Rev. A* **1992**, *46*, 2045.
(48) Jullien, R.; Botet, R. *Aggregation and Fractal Aggregates*; World Scientific: Singapore, 1987; p 88.
(49) Botet, R.; Jullien, R. *J. Phys. A: Math. Gen.* **1979**, *19*, L907.

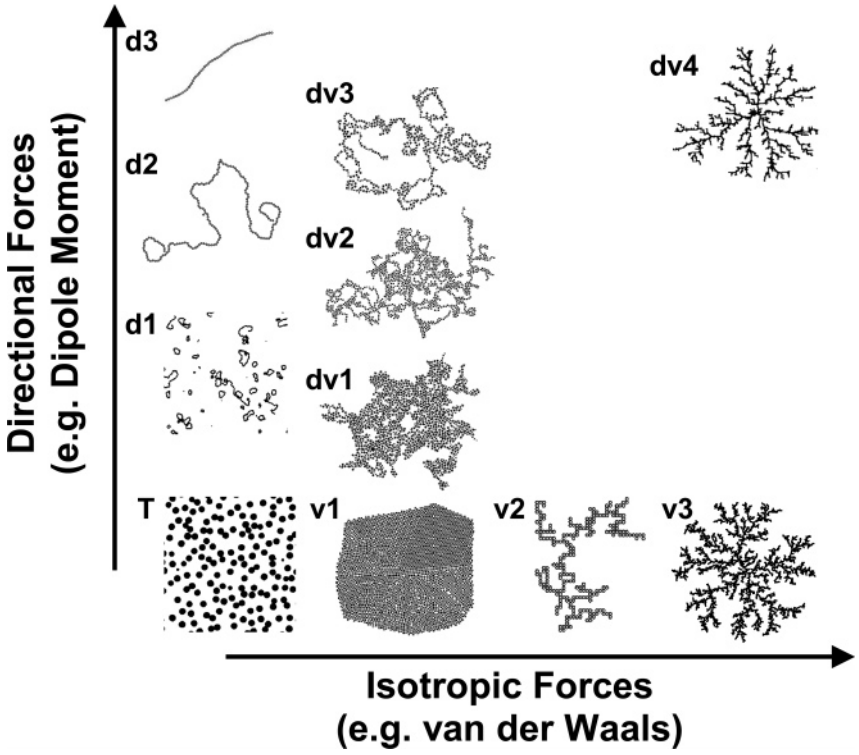

Figure 6. Schematic of aggregate morphology with respect to the strengths of the van der Waals interaction and dipolar interaction. Along the *x*-axis, one sees the competition between thermal energy and the van der Waals interaction. T shows a situation where thermal energy disperses the particles into a 2-D gas (Figure 2a), v1 shows equilibrium phase separation as depicted by our rule-based growth algorithm, v2 is an RLA simulation (ref 46), and v3 is a DLA simulation (ref 45). In terms of increasing the dipole moment, d1 is a Monte Carlo simulation of equilibrium polymerization taken from ref 61, d2 is from our rule-based growth simulation of a relatively strong dipolar attraction, and d3 is the same simulation in the limit of strong dipolar attraction. Finally, the competition between van der Waals attraction and dipolar attraction can be seen within the first quadrant of the graph. dv1, dv2, and dv3 were also generated by our rule-based simulation, and they show the effects of gradually increasing the dipolar attraction in the presence of weak to moderate van der Waals forces. The aggregate for dv4 was obtained from ref 44, and it corresponds to the case where both interactions are much greater than the thermal energy.

Table 1. Theoretical Predictions for the Fractal Dimension (d_f) and Aspect Ratio (A) for Particle Aggregates with Isotropic Interaction Potentials[47−49]

	DLCA	RLCA	phase separation
d_f	1.44	1.55	2
A	4.4	3.6	1

expected for phase separation. In contrast, the Au nanoparticles flocculated into highly branched structures and often had high aspect ratios. The typical values for d_f and A were near 1.67 and 4, respectively. Note the similarity with RLCA, and compare Figure 3 with the simulation labeled as v2 in Figure 6.

Also having noninteger values of d_f were aggregates of the CdTe quantum dots and magnetite nanoparticles. However, in this case, the particles do not simply flocculate. The particle organization is now significantly affected by their dipole moments. Experimental values of the dipole moment for II−VI-type semiconductor nanoparticles such as CdTe range from 1.3 to 3.3 $\times 10^{-28}$ C·m.[50,51] Additionally, a 25 nm magnetite particle has a magnetic dipole moment of roughly 2.5×10^{-18} A·m^2.[52,53] A pair of such particles in contact with aligned dipole moments would therefore bind with an energy of $\sim -2.3k_BT$ and $-19k_BT$, respectively.[54]

This addition of dipolar interactions relates to issue (2) listed above. To see the effects of this issue, refer to the morphological trends that develop along the *y*-axis in Figure 6. The morphology is now controlled by the competition between van der Waals and dipolar interactions (Figure 6 dv1, dv2, dv3, and dv4). Within the context of equilibrium particle aggregation, it is instructive to make a distinction between two types of aggregation: phase separation and equilibrium polymerization. Phase separation, for example, includes familiar processes such as the formation of liquid droplets from a vapor (Figure 6 v1). Equilibrium polymerization, on the other hand, applies to the stringlike self-organization of magnetic nanoparticles[55−57] and the formation of actin networks.[58,59] Unlike phase separation and flocculation,

(50) Blanton, S. A.; Leheny, R. L.; Hines, M. A.; Guyot-Sionnest, P. *Phys. Rev. Lett.* **1997**, *79*, 865.

(51) Shim, M.; Guyot-Sionnest, P. *J. Chem. Phys.* **1999**, *111*, 6955.

(52) The magnetic dipole moment (μ) for a particle of radius r, density ρ, and saturation magnetization σ_s is given by $\mu = {}^4/_3\pi r^3\rho\sigma_s$. A 25 nm magnetite particle with $\sigma_s = 60$ A·m^2/kg and $\rho = 5$ g/cm^3 would then have a magnetic dipole moment of roughly 2.5×10^{-18} A·m^2. Note that the saturation magnetization would be much lower if the magnetite has been oxidized to form maghemite. Such a change would not be unexpected when exposing magnetite nanoparticles to water, but the dipolar attraction would still be relatively large. For a measurement of σ_s, see ref 53.

(53) Lin, C.-R.; Chu, Y.-M.; Wang, S.-C. *Mater. Lett.* **2006**, *60*, 447.

(54) The interaction energy between a pair of magnetic dipoles is given by $E_{magdipole} = -1/(4\pi\mu_r\mu_0 r^3)[3(\vec{\mu}_1\cdot\hat{r})(\vec{\mu}_2\cdot\hat{r}) - \vec{\mu}_1\cdot\vec{\mu}_2] = -(2\mu^2)/(4\pi\mu_r\mu_0 r^3)$, where $\vec{\mu}_i$ is the dipole moment of particle i, μ_0 is the permeability of free space, μ_r is the relative permeability of water, $\vec{r}$ is the interparticle vector, r is the distance between the two particles in contact, and $\hat{r}$ is the unit vector equal to $\vec{r}/r$. The equation changes to $E_{eldipole} = -(2\mu^2)/(4\pi\epsilon_r\epsilon_0 r^3)$ for a pair of electric dipoles, where ϵ_0 is the permittivity of free space and ϵ_r is the dielectric constant of the medium. A pair of 25 nm magnetite nanoparticles in contact having aligned dipole moments would therefore bind with an energy of approximately $-19k_BT$. A pair of aligned CdTe quantum dots would bind with an energy of roughly $-2.3k_BT$. Note that $\mu_r\mu_0 = 1.26 \times 10^{-6}$ NA^{-2} (value for water) and $\epsilon_r = 41.6$ (average of water and DDMA) were used for these calculations.

(55) De Gennes, P. G.; Pincus, P. A. *Phys. Kondens. Mater.* **1970**, *11*, 189.

(56) Jordan, P. C. *Mol. Phys.* **1973**, *25*, 961.

(57) Butter, K.; Bomans, P. H. H.; Frederik, P. M.; Vroege, G. J.; Philipse, A. P. *Nat. Mater.* **2003**, *2*, 88.

(58) Pollard, T. D.; Cooper, J. A. *Annu. Rev. Biochem.* **1986**, *55*, 987.

(59) Disanza, A.; Steffen, A.; Hertzog, M. *Cell Mol. Life Sci.* **2005**, *62*, 955.

it is a true self-assembly process in which the blueprint for the final structure is coded within the interaction potential of the particles themselves.[29,30,60,61]

When the dipolar attraction dominates over these isotropic interactions, one would expect the particles to assemble into linear chains or loops (Figure 6 d1, d2, and d3). When dipolar forces are absent, one would expect disklike clusters due to the isotropic van der Waals potential (Figure 6 v1). The case of competing interaction potentials is the most common in our measurements (Figure 6 dv1, dv2, dv3, and dv4). It leads to intermediate structures such as highly branched chains and spongy networks. To gain insight into this general trend, we have written a simple program for generating 2-D aggregates using a rule-based growth algorithm. Essentially, the simulation starts with a single particle of radius 5 at the center of a 1000 × 1000 grid. When a particle is placed into contact with another particle in the growing aggregate, it can be placed either at the minimum of the local van der Waals potential or along the minimum of the local dipolar interaction potential. Since thermal energy is required to rotate the particle away from the dipole minimum, the particle is *not* placed along the direction of the dipole moment when

$$w \leq \exp[E_{\text{dipole}}/k_{\text{B}}T] \tag{2}$$

where w is a random number between 0 and 1 and E_{dipole} is the potential energy of two aligned dipoles in contact. Starting from a $0k_{\text{B}}T$ dipolar attraction and working up to a $-100k_{\text{B}}T$ dipolar attraction, the simulation results can be seen in v1, dv1, dv2, dv3, d2, and d3 of Figure 6. A more complete description of the simulation and the key results is given as Supporting Information (Figure S2).

The simulation essentially agrees with the experimental findings of this study: large dipole moments generate stringlike structures, while small dipole moments generate radially symmetric aggregates. This difference can be characterized by calculating d_{f} and A. Referring again to the two extreme cases, a disk-shaped cluster would have $d_{\text{f}} = 2$ and $A = 1$, and a straight linear chain would have $d_{\text{f}} = 1$ and $A = \infty$. Intermediate cases would, of course, have a fractal dimension between 1 and 2, with the proximity to 1 or 2 indicating the degree of self-assembly versus the degree of phase separation. Note the striking similarities between Figure 2b and Figure 6 v1, between Figure 4 and Figure 6 dv2, and again between Figure 5 and Figure 6 dv3. One may also compare Figure 6 d1 and d2 with the chainlike assemblies of cobalt nanoparticles observed in previous studies.[62−64]

Observe that care must be taken not to confuse self-assembled aggregates of dipolar particles with highly branched DLCA or RLCA aggregates (e.g., Figure 5 vs Figure 3). This situation is where the use of A is most helpful. No theoretical predictions for A are available for dipolar self-assembly, but the experimental and simulation results of this paper suggest that A will differ significantly from that expected for DLCA and RLCA aggregates with similar d_{f} values. Certainly, the morphology of linear chains that perform random walks has been analyzed in great detail.[65,66] Self-avoiding random walks in two dimensions have $d_{\text{f}} = 1.33$, and A is approximately equal to 5.8 according to the "asphericity" parameter.[67] Therefore, the *combination* of d_{f} and A makes it possible to distinguish between phase separation and branched polymer self-assembly based on image analysis alone. A more thorough investigation of this hypothesis is beyond the scope of this paper and will be considered in a future publication.

Conclusion

With the ability to visualize aggregation for a wide variety of materials under such similar conditions, the current platform provides experimental access to the full range of particle aggregation mechanisms: flocculation, phase separation, and self-assembly. Although the 1 s photopolymerization is not truly instantaneous, our evidence to this point is that the diffusion of the particles gradually slows and stops during the cure and that the polymerization does not bias the diffusion paths in such a way as to alter the final morphology of the aggregate. We have shown that nanoparticles will aggregate into a wide variety of complex morphologies and that the underlying mechanisms of aggregate formation can vary greatly despite superficial resemblance of the aggregates themselves. Although the agreement we find between our minimal model and experiment does not necessarily verify our hypothesis, it provides strong evidence for the importance of the asymmetric dipole interaction in generating the rich complexity of aggregate morphologies that were observed. Future studies will explore the competition between dispersion and dipolar interactions in more detail by systematically varying the magnetic dipole moments of the magnetite nanoparticles. We will further investigate the kinetics and reversibility of these processes by varying the temperature and by performing the flash cure at a series of different aggregation times. Having established this method, we hope to then extend these studies to other types of asymmetric potentials, such as quadrupoles and asymmetric repulsive potentials that arise simply from the irregular shapes of the building blocks.

Experimental Section

Sample Preparation. Figure 1 illustrates the experimental setup for performing 2-D particle aggregation. It consists of an oil phase, a water phase, and a solid support for the oil phase. To promote wetting and adhesion with the oil phase, clean glass slides were functionalized with 3-methacryloxypropyltrimethoxysilane (MPTMS, Aldrich[35]). Prior to deposition, a solution was prepared containing 135 mL of acetone, 15 mL of water, and 0.75 mL of MPTMS. The pH was then adjusted to 4 with HCl. The solution was allowed to stand for 1 h prior to deposition to allow for hydrolysis of the MPTMS. After immersing the glass slides in the solution for 10 min, they were quickly placed in an oven where they were cured for 1 h at 100 °C in air. The glass slides were then cleaned with soap and water to remove any excess silane.

The oil phase used for the self-assembly consisted of 1,12-dodecanediol dimethacrylate (DDMA) and 2 wt % Irgacure 819 (bis(2,4,6-trimethylbenzoyl)-phenylphosphineoxide, Ciba Specialty Chemicals[35]). Irgacure 819 is a particularly efficient photoinitiator, which is designed for the radical polymerization of acrylate monomers upon UV light exposure. At room temperature, water has a viscosity of 0.89 mPa·s and DDMA has a viscosity of 15 mPa·s. The interfacial tension between these two fluids is ~15 mJ/m^2 at 25 °C, which is of the same order as that between water and cooking oil.

(60) Stambaugh, J.; van Workum, K.; Douglas, J. F.; Losert, W. *Phys. Rev. E* **2005**, *72*, 031301.
(61) Tavares, J. M.; Weis, J. J.; Telo da Gama, M. M. *Phys. Rev. E* **2002**, *65*, 061201.
(62) Marin-Almazo, M.; Carcia-Gutierrez, D.; Gao, X.; Elechiguerra, J. L.; Kusuma, V. A.; Samon, W. M.; Miki-Yoshida, M.; Dalton, A. B.; Excudero, R.; Jose-Yacaman, M. *Nano Lett.* **2004**, *4*, 1366.
(63) Tripp, S. L.; Pusztay, S. V.; Ribbe, A. E.; Wei, A. *J. Am. Chem. Soc.* **2002**, *124*, 7914.
(64) We do not claim that our simulation describes equilibrium self-assembly, but the topological characteristics of these clusters are reproduced by our simple model. Van Workum and Douglas[29,30] have considered more complex algorithms that allow the computation of the fluid properties of self-assembling dipolar fluids with competing van der Waals interactions.
(65) Solc, K. *J. Chem. Phys.* **1971**, *55*, 335.
(66) Rudnick, J.; Gaspari, G. *J. Phys. A: Math. Gen.* **1986**, *19*, L191.
(67) Bishop, M.; Saltiel, C. J. *J. Chem. Phys.* **1988**, *10*, 6594.

When exposed to a 365 nm high-pressure mercury lamp at an intensity of 8 mW/cm^2, solidification of DDMA was achieved within 1 s. The aqueous phase was buffered using 10 mmol/L *N*-(2-hydroxyethyl)piperazine-*N*′-2-ethanesulfonic acid (HEPES, Aldrich[35]) and 100 mmol/L NaCl, and it was adjusted to a pH of 8. The relatively high salt concentration reduced the tendency of water to emulsify within the DDMA.

Since glass strongly absorbs UV radiation, the sample geometry was chosen so that the oil phase was immersed in the aqueous phase on the upper surface of the glass slide. This choice often led to dewetting, since both the three phase contact angle and lower density of the oil phase tended to remove the DDMA from the slide. These challenges were overcome by precuring a thin film ($\sim$100 μm) of poly(1,12-dodecanediol dimethacrylate) (PDDMA) on top of the methacrylate-functionalized surface. The self-wetting condition was subsequently found to be sufficient for maintaining the DDMA film (also $\sim$100 μm) in this configuration, even after immersion in water.

With respect to the self-assembly process, it was carried out by first dispersing the particles within either the oil or water phase. Depending upon the particle properties, they then segregate to the interface with a given association constant, *K*. One can therefore control the areal density of particles by controlling the bulk concentration of the particles in the suspension. Though kinetics play a large role in both the segregation and aggregation processes, the processing time (the time between initial immersion and UV flash curing) was generally chosen to produce similar particle densities for each material. The deposition time therefore varied from 15 to 60 min depending on the particle type. With this approach, the time resolution is limited primarily by the uncertainty of knowing the instant at which the oil phase comes into contact with water (the beginning of the experiment). The instant at which the UV irradiation commences, which can be easily controlled, produces an uncertainty of less than 1 s.

Since flash curing prevented further evolution of the aggregates at the interfaces, the polymerization resulted in a "snapshot" of the 2-D aggregation process at the moment when the DDMA was exposed to UV light. After removing the solidified samples from water and drying them, they could be conveniently inspected by a variety of microscopy techniques. The majority of the micrographs were obtained using a Digital Instruments[35] 3100 atomic force microscope (AFM) in tapping mode. Larger particulate aggregates were inspected using a Nikon[35] Optiphot-2 light optical microscope (LOM).

Acknowledgment. Fellowship support from the National Research Council is gratefully acknowledged. We also acknowledge Eric Amis from the Polymers Division at NIST for support of the project and for his helpful input with regard to this paper. In addition, we thank Joe Antonucci, Hua Hu, and Steve Hudson from the Polymers Division at NIST for providing resources and for their helpful discussions.

Supporting Information Available: Optical micrographs of 25 nm magnetite nanoparticle aggregates and representative simulation results for the rule-based growth of identical particles of radius 5 on a 1000 $\times$ 1000 array. This material is available free of charge via the Internet at http://pubs.acs.org.

LA062230I